NANO LETTERS

LETTER

pubs.acs.org/NanoLett

Size-Dependent Electron Transfer from PbSe Quantum Dots to SnO_2 Monitored by Picosecond Terahertz Spectroscopy

Enrique Cánovas,*[,†] Puck Moll,[†] Søren A. Jensen,[†] Yunan Gao,[‡,§] Arjan J. Houtepen,[‡] Laurens D. A. Siebbeles,[‡] Sachin Kinge,*[,∥] and M. Bonn[†,⊥]

[†]FOM Institute for Atomic and Molecular Physics, Science Park 104, 1098 XG Amsterdam, The Netherlands

[‡]Chemical Engineering, Delft University of Technology, Julianalaan 136, 2628 BL Delft, The Netherlands

[§]Kavli Institute of Nanoscience, Delft University of Technology, Lorentzweg 1, 2628 CJ Delft, The Netherlands

[∥]Materials Research and Development, Toyota Europe, Hoge Wei 33, B-1930. Zaventem, Belgium

[⊥]Max Planck Institute for Polymer Research, Ackermannweg 10, 55128 Mainz, Germany

Supporting Information

ABSTRACT: We report the direct and unambiguous determination of electron transfer rates and efficiencies from PbSe quantum dots (QDs) to mesoporous SnO_2 films. We monitor the time-dependent electron density within the oxide with picosecond time resolution using Terahertz spectroscopy, following optical excitation of the QDs using a femtosecond laser pulse. QD-oxide electron transfer occurs with efficiencies of ∼2% in our samples under 800 nm pumping with a marked dependence on QD size, ranging from ∼100 ps injection times for the smallest, ∼2 nm diameter QDs, to ∼1 ns time scale for ∼7 nm QDs. The size-dependent electron transfer rates are modeled within the framework of Marcus theory and the implications of the results for device design are discussed.

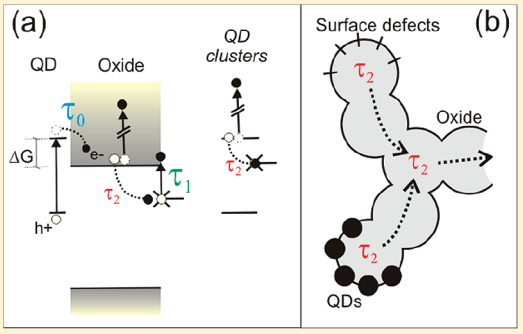

KEYWORDS: QD sensitized solar cell, THz spectroscopy, electron transfer, Marcus theory, PbSe QDs

In 1991 O'Regan and Grätzel presented a new route for the development of efficient low cost photovoltaic devices based on dye-sensitized colloidal TiO_2 films[1] (dye sensitized solar cells, DSSCs). Later on, the unique properties of semiconductor nanocrystals (quantum dots, QDs) prompted efforts to substitute the dyes by QD absorbers as a way of optimizing those devices.[2−4] However, although the tunable absorption edge of QDs and their larger absorption cross sections seemed to provide the QDs an advantage over the dyes, for example, in enabling to better match the solar spectrum, the reported power conversion efficiencies of QD sensitized solar cells[5] (QDSSCs) have remained limited to 4−5%. This is clearly not competitive with figures obtained for DSSCs reaching values up to 11%.[6] Reasons like the nonhomogeneous sensitization of the oxides by QDs, the presence of QD surface defects, and the employment of electrolytes less compatible with QDs, have been proposed in order to explain the gap in efficiencies between both technologies.[7] While quantum efficiency measurements on complete QDSSC devices enable quantification of their performance, such measurements are unable to resolve which physical process in the device is limiting its overall efficiency. For example, reduced photocurrent in devices can be caused by inefficient electron transfer from the QD donor to the oxide acceptor, electron capture (trapping) in the oxide contact or a bad performance of the electrolyte. In order to identify the bottleneck, it is essential to obtain information about the efficiency and time scales of fundamental processes taking place in the devices. In this paper, we will focus on the understanding of electron transfer (ET) phenomena occurring after photoexcitation from the QDs (donors) to the oxide film (acceptor).

The most common employed techniques which are used to interrogate ET processes before device encapsulation are photoluminescence (PL) and transient absorption (TA) spectroscopy. These techniques probe carrier populations within the QDs. The reduction of QD luminescence[4,8] or increase in absorption[9] signals after their attachment to the oxide film has been employed to monitor carrier transfer between the species. However, the disappearance of charge carriers from the QD does not always necessarily imply that they have been transferred to the oxide. New recombination pathways for electrons within the QDs after the oxide sensitization may occur (e.g., changes in the QD surface chemistry after attachment). Given that the spectroscopic signature of ET and that associated with trapping processes within the QD are identical, it is not straightforward to differentiate between the two proccesses, unless additional measurements are performed (e.g., photocurrent on devices). Indeed, such loss channels, and the associated breakdown of correlation between optical signatures and electron transfer, have been identified for

Received: July 26, 2011
Revised: October 26, 2011
Published: October 31, 2011

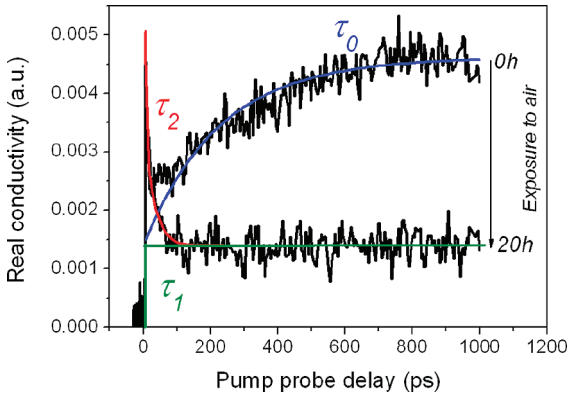

Figure 1. Characteristic carrier dynamics monitored by THz-TDS on PbSe QDs sensitizing SnO_2 film before (0 h) and after (20 h) exposing the sample to air. The highlighted time constants (τ_0, τ_1, and τ_2) are correlated with three different mechanisms discussed in the text.

CdSe QDs sensitizing SiO_2[9] and PbSe QDs sensitizing TiO_2.[10] In both systems, the transient optical signals can be fully accounted for by defect-related recombination within the QDs after oxide sensitization.

Terahertz time domain spectroscopy[11] (THz-TDS) has previously been shown to be a useful tool to monitor unambiguously ET between the QD donor and the oxide acceptor.[10] This technique is unique as it can probe the photoconductivity in the oxide film after selective QD photoexcitation. The probing THz field (0−8 meV) provides a means to perform an ultrafast, contact-free conductivity measurement. As long as the charge carriers remain localized in the QD, there is no real conductivity, but the THz field interacts strongly with free electrons populating the oxide conduction band. In this respect, THz-TDS, in contrast to optical probes, can provide unambiguous information about ET rates on QDs sensitizing oxide surfaces. The sample under study is optically photoexcited by a 800 nm femtosecond laser pulse (pump beam). Just after photoexcitation, the time-dependent conductivity within the oxide is monitored by a terahertz field (probe) with picoseconds time resolution. The time-dependent conductivity signal is directly proportional to the product of electron density and mobility within the mesoporous oxide. Details about the THz-TDS setup, THz measurements, and sample preparation are given in the Supporting Information.

Colloidal PbSe QDs sensitizing SnO_2 mesoporous films were studied in this work to probe ET dynamics in QD-oxide systems. The bifunctional molecule MPA (mercapto propionic acid) was employed to anchor the QD donors to the oxide acceptor. Our motivation for studying this system is two-fold: SnO_2 is a better conductor than, for example, the broadly studied TiO_2, and lead salt-based QDs have been pointed as excellent candidates for solar energy conversion[12] due to their tunable bandgap covering IR and visible wavelengths.

Figure 1 shows the carrier dynamics monitored by THz-TDS for a sample consisting of PbSe QDs sensitizing SnO_2 mesoporous film before (0 h) and after 20 h of air exposure. Before air exposure (0 h trace in Figure.1) the carrier dynamics are governed by two components, a "fast" decay (τ_2, recombination process) and a "slow" (τ_0 in Figure.1) ingrowth. The slow ingrowth is attributed to ET from the QD to the oxide, but the fast decay appears as a parasitic unexpected signature in the carrier dynamics. More information about the different carrier dynamics processes can be obtained by exposing the colloidal QDs to air (oxidation), which has dramatic effects on their optical properties.[13−15] Oxidation causes the QD protecting ligands to be removed, providing new nonradiative relaxation pathways for the photogenerated e−h pairs. The resulting QD surface traps will greatly reduce the chance for electrons to be transferred to the oxide (electron trapping within the QD will compete efficiently with ET). We can thus take advantage of the oxidation phenomena in order to discriminate between ET and parasitic signals. As shown in Figure 1, after 20 h of exposing the sample to air, the slow ingrowth component (blue trace) has vanished, indicating that the τ_0 component is related with ET from the QDs to the mesoporous oxide. For the oxidized sample (20 h in Figure 1), two components are resolved after time zero (0 ps in Figure 1), the fast recombination process (τ_2, red line) resolved also before oxidation and a long-time offset (τ_1, green line). In a previous publication, we attributed these parasitic signals to electron transfer within QD clusters,[10] but we will show here that other explanations are also possible and perhaps more plausible. The measurement of a sample consisting on drop-casted QDs exposed to air (Supporting Information, Figure S2) provides dynamics that are compatible with the detected fast recombination component (τ_2, red line) at short time scales but do not exhibit conductivity at long times assigned as the τ_1 component (green line in Figure 1). Hence, the fast recombination process and the long-lived signals seem to originate from two different mechanisms. A simple mechanism that can explain the τ_1 signal is the generation of new defect states in the SnO_2 surface induced by the presence of the PbSe QDs (e.g., direct attachment of dots to the oxide phase). The subpicosecond ingrowth after photoexcitation (τ_1 component) is then related to photoexcitation of electrons from these surface defect states to the oxide CB. Reference measurements on bare SnO_2 and SnO_2 + MPA mesoporous films did not reveal any real conductivity under the same 800 nm pump (there are no shallow donors before QD attachment), corroborating that the detected ultrafast τ_1 signal is induced after the QD attachment (defect related injection). Interestingly, similar ultrafast carrier dynamics components have been also reported for dye-oxide sensitization. Subpicosecond signals have been attributed to hot carrier injection effects[16] or to the presence of dye induced surface defect traps[17] acting as a pathway for electron injection in the oxide. Although QD and dye systems are intrinsically different, it is worth noting that the latter scenario is identical to the defect-assisted injection giving rise to the long-time conductivity concluded for the QD-oxide system.

Fluence dependent measurements on PbSe+SnO_2 samples exposed to air (Supporting Information, Figure S3) suggest that the parasitic τ_2 component is related to a trap-assisted Auger recombination process[18] (the lifetime depends inversely on carrier density, $\tau_2 \propto 1/n$). Auger recombination has been reported to govern the carrier dynamics in both mesoporous oxide films[19] and QD supperlatices.[20] Accordingly, we can relate our measured fast recombination process with trapping of free electrons populating the oxide or/and trapping within QD aggregates (clusters[10]) present in the samples. Direct evidence of clustering formation in our samples was obtained by structural characterization (Supporting Information, Figure S4).

The strength of the Auger recombination signal was noticed to depend on the probed area (Supporting Information, Figure S5), indicating local variations of carrier relaxation strength within the oxide and/or an inhomogeneous distribution of clustered phases across the sample. If the detected Auger recombination happens

dx.doi.org/10.1021/nl202550v |*Nano Lett.* 2011, 11, 5234–5239

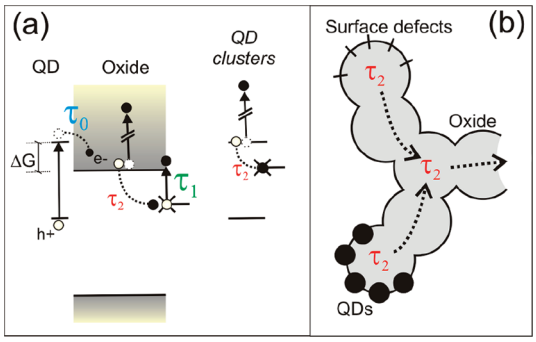

Figure 2. (a) Proposed scenario describing contributions to the carrier dynamics measured by THz-TDS on PbSe sensitizing mesoporous SnO_2. τ_0 refers to the electron transfer from isolated QDs first excite state to the oxide CB (defined by ΔG); τ_1 refers to electron injection from surface defect states to the oxide CB; τ_2 refers to trap-assisted Auger recombination within the oxide nanoparticles and/or within QD clusters. (b) Auger recombination (τ_2) can be enhanced locally in the oxide due to an inhomogeneous distribution of donor phases (τ_0 and τ_1) and/or bottlenecks for current extraction.

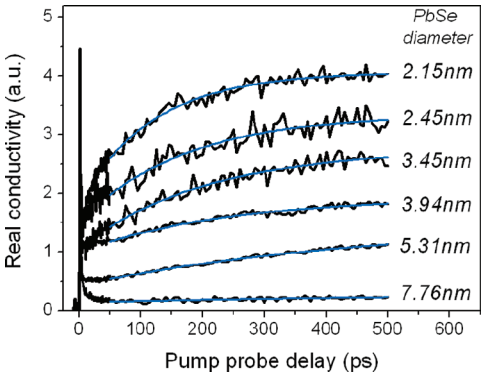

Figure 3. QD size-dependent electron transfer monitored by THz-TDS on PbSe QDs sensitizing SnO_2 films. Blue lines show a single-exponential increase in the conductivity. Different traces are multiplied by different factors for comparison purposes.

within the oxide, the local variations are indicative of different local concentration of anchored QDs (by MPA) and/or QD induced surface defects that can enhance the generation of bottlenecks for current flow within the oxide matrix (enhancing Auger recombination). On the other hand, if the fast Auger recombination is purely related to the presence of QD clusters, their inhomogeneous distribution across the samples can be the result of local chemical degradation of the clusters because of the presence of water[13] and/or an excess of MPA,[21] or physically by the nonefficient penetration of the QDs in the porous oxide films promoting QD aggregation[7,22] (Supporting Information, Figure S4). Whatever the origin of the observed fast recombination, the use of oxide materials with a smaller surface-to-volume ratio (such as "thick" nanowires) will in principle prevent its appearance in the samples, avoiding bottlenecks for current flow and homogenizing the amount of attached dots per unit area.

Figure 2a summarizes the different mechanisms (from τ_0 to τ_2) involved in the time-resolved conductivity signals for PbSe QDs sensitizing SnO_2 films as discussed before. The τ_0 component results from ET processes from PbSe QDs to the SnO_2 film; the τ_1 signal results from the presence of oxide surface states promoted by the attachment of QDs; and the τ_2 component comes from QD clusters and/or bottlenecks for current flow within the oxide. In Figure 2b is shown how the Auger recombination processes (τ_2) can arise from an inhomogeneous distribution of electron donor phases (anchored QDs or surface states) promoting bottlenecks for the current flow. Note that, although from different origins, the mechanisms τ_0 and τ_1 will contribute both to the photocurrent on QDSSCs devices.

From our measurements we can obtain an estimate for the efficiency of the ET process (under 800 nm photoexcitation) between the QD donor and oxide acceptor in our samples by the following simple comparison:

$$\text{Efficiency}_{ET} = \frac{\text{Conductivity}(\text{PbSe} + \text{SnO}_2)}{\text{Conductivity}(\text{SnO}_2)} \qquad (1)$$

Where Conductivity(PbSe+SnO_2) and Conductivity(SnO_2) refers to the measured real conductivity amplitude signals in the QD sensitized sample (Figure 1, when reaching the plateau value at 1 ns) and a SnO_2 reference sample with known excitation density due to direct excitation from the valence band (amplitude just after photoexcitation with 266 nm light). From eq 1, a value of $\text{Efficiency}_{ET} = 2.0 \pm 0.6\%$ was obtained when considering only the amplitude relative to the pure ET process (τ_0 in Figure 1). The efficiency reaches values of $3.7 \pm 0.6\%$ when also the τ_1 process (Figure 1) is considered. The error bar accounts for the measured locally variations in the real conductivity amplitudes across the samples. These modest figures cannot be considered as an intrinsic feature of the PbSe + SnO_2 system but as a result coming from our particular samples, where presumably an excess of QDs (clustered and nonlinked to the oxide surface, Supporting Information, Figure S4) are responsible for the high photon absorption and small electron transfer efficiency.

Having identified unambiguously the τ_0 component as the QD-oxide ET time, we determine the QD size dependence of ET rates in these systems. Figure 3 shows the real conductivity (proportional to the free carrier concentration) versus pump−probe delay (temporal window between 0 and 500 ps) for a set of 6 PbSe QD sizes (diameters from 2.15 to 7.76 nm). In order to extract the ET rate constants from the QDs to the oxide (τ_0 in Figures 1 and 2), we describe the data using the following equation:

$$\sigma_{\text{real}}(t) \sim N(t) = N_0\left[1 - \exp\left(-\frac{t}{\tau_0}\right)\right] + y_1 \qquad (2)$$

Where $N(t)$ represents the amount of free carriers in the samples as a function of time, $(1/\tau_0) = k_0$ is the rate constant for the ET between QD and oxide and y_1 is a DC offset representing the contribution from the τ_1 mechanism (Figures 1 and 2). Data from 50 ps onward were considered (blue traces in Figure 3) to reduce complications due to contributions from Auger recombination, which is largely complete by that time. The simple, single-exponential ingrowth model (eq 2) reproduces the data remarkably well; there are no grounds for using several and/or stretched exponentials (see below). The single exponential fitting indicates a high degree of homogeneity in the attached QD, in terms of both the average distance between the dot and the oxide (defined by the MPA linker) and QD size (determining the relative band alignment between donor and acceptor, ΔG in Figure 2). Direct evidence for the latter was obtained by transmission electron microscopy (TEM) analysis on the samples (Supporting Information, Figure S4). We find no evidence for significant hot ET

dx.doi.org/10.1021/nl202550v |Nano Lett. 2011, 11, 5234–5239

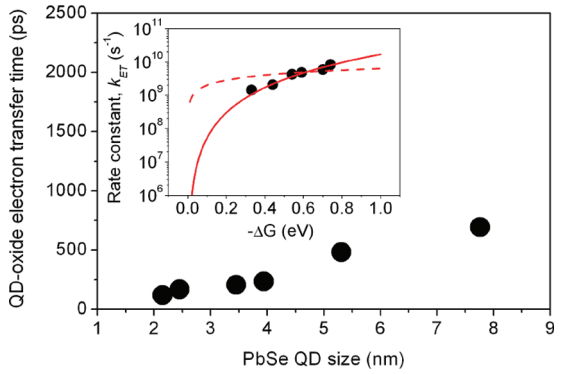

Figure 4. QD size-dependent electron transfer lifetime for PbSe dots anchored to SnO_2 by MPA. The inset depicts the corresponding rate constants as a function of the relative band alignment (ΔG) between donor and acceptor species; the solid (dashed) red line is the best fit following many-states Marcus theory when considering a quadratic (constant) dependence on energy for the wave function overlap between the QD and the oxide (see text for details).

(electron transfer from QD levels above the QD first excited state), as previously reported[23] for PbSe QDs sensitizing TiO_2.

Figure 4 shows the QD-oxide ET times as a function of QD diameter obtained from the model shown as blue lines in Figure 3 (numbers are also included in Table 1). Within the investigated QD size range, a more or less linear dependence is obtained. These results explain why a single exponential fitting (by eq 2) provides an adequate model for the ET processes observed in our samples (see Figure 3). A characteristic broadening of ~60 meV for the first QD absorption peak in our samples was measured by optical spectroscopy. From this broadening we can infer a variation in size of our QDs of around 5% (in agreement with TEM observations, Supporting Information Figure S4). According to the results shown in Figure 4, such a variation in QD size would result in a variation in injection rates of ±16 ps which is not enough to be reflected in the carrier dynamics given the limited signal-to-noise ratio of our measurements (see error bars in Table 1).

Electron transfer processes between two discrete energy states can be modeled by the Marcus theory.[24] This theory has been extended for describing electron transfer processes taking place in systems were the acceptor is defined by a continuum of states, as occurs in dye-[25] and QD-[9] sensitized oxides. Accordingly, our monitored QD size-dependent ET rate can be modeled as follows:

$$k_{ET} = \frac{2\pi}{\hbar}\int_{-\infty}^{\infty} dE\rho(E)|H_{AB}(E)|^2 \frac{1}{\sqrt{4\pi\lambda k_B T}} \exp\left(-\frac{(\lambda + \Delta G + E)^2}{4\lambda k_B T}\right) \quad (3)$$

Where k_{ET} is the transfer rate constant between donor and acceptor species which is governed by (i) the density of accepting states in the oxide $\rho(E)$, (ii) the distance between donor and acceptor (defining the wave function overlap, $|H_{AB}(E)|^2$), (iii) the energy difference between donor and acceptor energy levels (defined by ΔG, Figure 2a), and (iv) the reorganizational energy (λ). Most of these parameters can be or have been determined independently. The density of states $\rho(E)$ near the oxide band edge can be described by a $E^{1/2}$ dependence[25] and the values for the relative band alignment between donor and acceptor (ΔG included in Table 1, see Figure 2a) can be estimated according to

Table 1. Electron Transfer (τ_0) Times, Rate Constants (k_{ET}), and Relative Band Alignment (ΔG) between QD Donor and SnO_2 Acceptor As a Function of PbSe QD Diameter[a]

QD diameter (nm)	ET time τ_0 (ps)	rate constant k_{ET} (s^{-1})	ΔG (eV)
2.15	120 ± 8	8.33×10^9	0.74
2.45	170 ± 25	5.91×10^9	0.70
3.45	210 ± 25	4.83×10^9	0.59
3.94	235 ± 25	4.27×10^9	0.54
5.31	480 ± 40	2.07×10^9	0.44
7.76	700 ± 1100	1.44×10^9	0.33

[a] $\Delta G = [LUMO_{QD} - CB_{oxide}]$ values were estimated attending to the reported QD and oxide alignments versus vacuum.[26,27]

their respective alignments versus vacuum.[26,27] The reorganizational energy (λ) that accounts for energy fluctuations in the system due to the charge transfer, has been reported to have characteristic small values of tens of millielectronvolts between nanocrystals[9,28] (with only passivating QD surface ligands or vibrational modes contributing to λ). The wave function overlap $|H_{AB}(E)|^2$ between donor and acceptor has been approximated as an energy-independent constant in previous works.[9,25] However, a more realistic energy dependence of the wave function overlap function between the QD and the oxide CB would have to take into account that the degree of electronic coupling is dependent on the leakage of the electron wave function outside the QDs. This has been shown to be larger for smaller QDs (stronger confinement) following a quadratic relationship with energy.[29] Accordingly, we have approximated the wave function overlap between the QD and the oxide CB as $|H_{AB}(E)|^2 \propto E^2$. In the inset of Figure 4, the solid line shows the best fitting obtained (with $\lambda = 1 \pm 50$ meV) when including the quadratic energy dependence of the wave function overlap due to QD quantum confinement. Apart from a scaling factor, the obtained description is in good agreement with the experimental data, showing the importance of the wave function overlapping contribution in the ET rates for the system under study. The dashed line (inset Figure 4) shows the same model assuming that $|H_{AB}(E)|^2$ is energy independent. We note that quantum confinement and hence wave function leakage in PbSe dots is particularly strong due to its big Bohr radius.[12]

Future analysis on the ET rates for different quantum dot-oxide material configurations, its dependence on the electron donor−acceptor separation (by employing bifunctional linkers of different length) and its dependence on the surrounding hole acceptor phase may further clarify the complex physicochemical processes governing ET in QDSSCs.

From the results presented above, we can draw some conclusions on their implications for solar cell device performance. Ultimately the potential of a QD sensitized solar cell for producing photocurrent hinges on how efficiently ET occurs. As shown above, using THz-TDS we are able to quantify the efficiency of the ET process in QD sensitized oxides. For our particular samples we obtained efficiencies of few percents in the ET process under 800 nm excitation. These modest figures cannot be considered as an intrinsic feature of the PbSe + SnO_2 system but as a particular result coming from our samples. The small ET efficiency (corrected for photon absorption efficiency) can presumably be traced to the presence of QDs with a high concentration of surface defects (killing ET efficiency as shown in Figure 1 for oxidized samples) and/or by the presence

dx.doi.org/10.1021/nl202550v |Nano Lett. 2011, 11, 5234–5239

of QD aggregates responsible for the high absorption and small ET efficiency (after photoabsorption the ET process take place between QDs, τ_2 in Figures 1 and 2, and not from QDs to the oxide).

The presence of QD clusters has been resolved in our samples by TEM measurements and is compatible with the measured ultrafast decay component in the carrier dynamics for QD sensitizing oxides (Supporting Information, Figure S4). As mentioned above, one simple route to prevent QD aggregation is to employ oxide geometries with a smaller surface-to-volume ratio, promoting a homogeneous distribution of attached dots per unit area. On the other hand, if QD clustering formation is unavoidable when sensitizing oxides, we have to try to take profit from its presence in future devices. One route to do so can be the modification of surface chemistry of the dots. This approach has been shown to enhance QD coupling in QD superlatices[30,31] and hence long-range electron transport among QDs. By using the same strategy when sensitizing oxides we can force our QD clusters to contribute to the injection of eletrons into the oxide. In other words, not only QDs directly contacted to the oxide will contribute to the solar cell photocurrent.

Finally, from the QD size-dependent analysis we have observed that ET is directly correlated with the energy difference between donor and acceptor levels (ΔG, Figure 2a) as Marcus theory predicts. The faster ET processes, a priori a desirable situation for solar cell performance, is achieved by the bigger ΔG values (in our system, ET occurs on ~100 ps for $\Delta G \sim 700$ meVs, see Table 1). However, while larger ΔG values will serve to increase the current, the device potential will be reduced in proportion to ΔG.[32] All things considered, the route to achieving the best efficiency in QD sensitized solar cells is by selecting the QD size with the slowest ET time (smallest ΔG) compatible with the rest of the kinetic processes taking place within the QDs (recombination processes within the QDs and QD regeneration by the electrolyte). Additionally, ET processes can be enhanced for a fixed ΔG by reducing the distance between donor and acceptor species (i.e., by changing surface ligands or by direct growth of the QDs onto the oxide).

In conclusion, we employed THz-TDS as a unique tool for the direct and unambiguous determination of electron transfer rates and efficiencies from PbSe QDs to mesoporous SnO_2. Also, we propose a single route to discriminate among the detected mechanisms in the carrier dynamics consisting on measuring the samples before and after sample's air exposure (oxidation process). By doing so, we observed that the electron population in the oxide CB after selective photoexcitation of the QDs is contributed by surface defect states induced by the QD sensitization that are inhomogeneously distributed across the oxide films. It was further shown that the population of electrons in the oxide CB could be limited by trap-assisted Auger recombination. We analyzed the ET rates (with efficiencies ~2% in our samples) as a function of QD size for the PbSe + SnO_2 system and discussed our results within the Marcus theory framework showing that small reorganizational energies can be characteristic for these systems. Finally, we draw some implications for realizing devices, highlighting that the payback for achieving ultrafast electron transfer processes is the reduction of the potential output solar cell voltage. In this respect, slower ET processes (due to reduced ΔG values) compatible with QD regeneration and electron transport are desirable for achieving higher efficiency in future devices.

■ ASSOCIATED CONTENT

Supporting Information. Preparation of PbSe QDs, preparation of QD PbSe sensitized SnO_2 films, description of THz-TDS setup and measurements, carrier dynamics of dropcasted PbSe QDs versus oxidized PbSe + SnO_2 sample, THz-TDS fluence dependent measurements on oxidized PbSe + SnO_2 sample, structural characterization of PbSe + SnO2 samples, THz-TDS measurements on different sample's spots for a PbSe + SnO_2 sample. This material is available free of charge via the Internet at http://pubs.acs.org.

■ AUTHOR INFORMATION

Corresponding Author

*E-mail: (E.C.) canovas@amolf.nl; (S.K.) Sachin.Kinge@toyota-europe.com.

■ ACKNOWLEDGMENT

This work has been financially supported by Toyota Motor Europe NV/SA and by the Nederlandse Organisatie voor Wetenschappelijk Onderzoek (NWO) within the research program "Stichting voor Fundamenteel Onderzoek der Materie (FOM)". A.J.H. acknowledges the 3TU Centre for Sustainable Energy Technologies (Federation of the Three Universities of Technology) for financial support.

■ REFERENCES

(1) O'Reagan, B.; Gratzel, M. *Nature* **1991**, *353*, 737.
(2) Zaban, A.; Micic, O. I.; Gregg, B. A.; Nozik, A. J. *Langmuir* **1998**, *14*, 3153.
(3) Vogel, R.; Hoyer, P.; Weller, H. *J. Phys. Chem.* **1994**, *98*, 3183.
(4) Gopidas, K. R.; Bohorquez, M.; Kamat, P. V. *J. Phys. Chem.* **1990**, *94*, 6435.
(5) Mora-Sero, I.; Bisquert, J. *J. Phys. Chem. Lett.* **2010**, *1* (20), 3046 and references therein.
(6) Chiva, Y.; Islam, A.; Watanabe, Y.; Komiya, R.; Koide, N.; Han, L. *Jpn. J. Appl. Phys.* **2006**, *45*, L638.
(7) Hodes, G. *J. Phys. Chem. C* **2008**, *112*, 17778.
(8) Blackburn, J. L.; Selmarten, D. C.; Nozik, A. J. *J. Phys. Chem. B* **2003**, *107*, 14154.
(9) Tvrdy, K.; Frantsuzov, P. A.; Kamat, P. V. *Proc. Natl. Acad. Sci. U.S.A.* **2011**, *108* (1), 29.
(10) Pijpers, J. J. H.; Koole, R.; Evers, W. H.; Houtepen, A. J.; Boehme, S.; de Mello-Donega, C.; Vanmaekelbergh, D.; Bonn, M. *J. Phys. Chem. C* **2010**, *114*, 18866.
(11) Ulbricht, R.; Hendry, E.; Shan, J.; Heinz, T. F.; Bonn, M. *Rev. Mod. Phys.* **2011**, *83* (2), 543.
(12) Wise, F. W. *Acc. Chem. Res.* **2000**, *33*, 373.
(13) Sykora, M.; Koposov, A. Y.; McGuire, J. A.; Schulze, R. K.; Tretiak, O.; Pietryga, J. M.; Klimov, V. I. *ACS Nano* **2010**, *4*, 2021–2034.
(14) Chappell, H. E.; Hughes, B. K.; Beard, M. C.; Nozik, A. J.; Johnson, J. C. *J. Phys. Chem. Lett.* **2011**, *2*, 889.
(15) Blackburn, J.; Chappell, H.; Luther, J. M.; Nozik, A. J.; Johnson, J. C. *J. Phys. Chem. Lett.* **2011**, *2*, 599.
(16) Benko, G.; Kallioinen, J.; Korppi-Tommola, J. E. I.; Yartsev, A. P.; Sundstrom, V. *J. Am. Chem. Soc.* **2002**, *124* (3), 489.
(17) Haque, S. A.; Palomares, E.; Cho, B. M.; Green, A. N. M.; Hirata, N.; Klug, D. R.; Durrant, J. R. *J. Am. Chem. Soc.* **2005**, *127*, 3456.
(18) Landsberg, P. T. *Phys. Status Solidi B* **1970**, *41*, 457.
(19) Cavaleri, J. J.; Colombo, D. P.; Bowman, R. M. *J. Phys. Chem. B* **1998**, *102* (8), 1341.
(20) Murphy, J. E.; Beard, M. C.; Nozik, A. J. *J. Phys. Chem. B* **2006**, *110*, 25455.

(21) We have noticed that the addition of MPA to QDs dispersed in toluene produces the aggregation of them (clustering formation).
(22) Guijarro, N.; Lana-Villareal, T.; Mora-Sero, I.; Bisquert, J.; Gomez, R. *J. Phys. Chem. C* **2009**, *113*, 4208.
(23) Tisdale, W. A.; Williams, K. J.; Timp, B. A.; Norris, D. J.; Aydil, E. S.; Zhu, X. Y. *Science* **2010**, *328*, 1543.
(24) Marcus, R. A. *J. Chem. Phys.* **1956**, *24*, 966.
(25) Sakata, T.; Hashimoto, K.; Hiramoto, M. *J. Phys. Chem.* **1990**, *94*, 3040.
(26) Hagfeldt, A.; Gratzell, M. *Chem. Rev.* **1995**, *95*, 49.
(27) Choi, J. J.; Lim, Y. F.; Santiago-Berrios, M. E.; Oh, M.; Hyun, B. R.; Sun, L.; Bartnik, A. C.; Goedhart, A.; Malliaras, G. G.; Abruña, H. D.; Wise, F. W.; Hanrath, T. *Nano Lett.* **2009**, *9* (11), 3749.
(28) Scholes, G. D.; Jones, M.; Kumar, S. *J. Phys. Chem. C* **2007**, *111*, 13777.
(29) Koole, R.; Liljeroth, P.; de Mello Donega, C.; Vanmaekelbergh, D.; Meijerink, A. *J. Am. Chem. Soc.* **2006**, *128*, 10436.
(30) Kovalenko, M. V.; Scheele, M.; Talapin, D. V. *Science* **2009**, *324*, 1417.
(31) Talapin, D. V.; Murray, C. B. *Science* **2005**, *310*, 86.
(32) Giebink, N. C.; Wiederrecht, G. P.; Wasielewski, M. R.; Forrest, S. R. *Phys. Rev. B* **2011**, *83*, 195326.